Evaluation of a Variable-Impedance Ceramic Matrix Composite Acoustic Liner

M. G. Jones*, W. R. Watson†, D. M. Nark‡, and B. M. Howerton§
NASA Langley Research Center, Hampton, VA 23681

As a result of significant progress in the reduction of fan and jet noise, there is growing concern regarding core noise. One method for achieving core noise reduction is via the use of acoustic liners. However, these liners must be constructed with materials suitable for high temperature environments and should be designed for optimum absorption of the broadband core noise spectrum. This paper presents results of tests conducted in the NASA Langley Liner Technology Facility to evaluate a variable-impedance ceramic matrix composite acoustic liner that offers the potential to achieve each of these goals. One concern is the porosity of the ceramic matrix composite material, and whether this might affect the predictability of liners constructed with this material. Comparisons between two variable-depth liners, one constructed with ceramic matrix composite material and the other constructed via stereolithography, are used to demonstrate this material porosity is not a concern. Also, some interesting observations are noted regarding the orientation of variable-depth liners. Finally, two propagation codes are validated via comparisons of predicted and measured acoustic pressure profiles for a variable-depth liner.

I. Introduction

A significant desire for reduced aircraft noise in the vicinity of airports has led the International Civil Aviation Organization (ICAO) and Federal Aviation Administration (FAA) to impose increasingly stringent aircraft noise requirements. In response to these requirements, one of the key components of NASA's Fundamental Aeronautics Program is to develop innovative aircraft noise reduction technology that could be used to meet these requirements. Aircraft noise can conveniently be divided into two components, propulsion noise and airframe noise. Of these, propulsion noise is dominant for the takeoff condition, and is similar in magnitude with airframe noise for the approach condition.[1]

Aircraft propulsion noise can be further separated into contributions due to the jet, fan and core. Historically, much of the research has concentrated on the jet and fan noise contributions, as they are typically much larger than the noise attributed to the core. However, sufficient progress has been made to reduce jet and fan noise levels such that the core noise contribution deserves greater attention. One option for core noise reduction is to use acoustic liners embedded within the interior walls of the core.

Clearly, a liner placed within the core will be exposed to much higher temperatures than those experienced in the bypass duct. Hence, acoustic liners constructed with conventional materials (typically, metallic or phenolic core with metallic or conventional composite facesheet) cannot be used for this application. Instead, one possibility is to use a liner constructed with ceramic matrix composite (CMC) material. However, the CMC material has a porosity of about 20%, and there is concern that this might affect the predictability of liners constructed with this material. Tests are needed to investigate this issue. Also, the main contributors to core noise (combustion noise and turbine fan noise) combine to form a broadband noise spectrum. Thus, the optimum liner configuration should be designed for broadband noise reduction.

*Senior Research Scientist, Research Directorate, Structural Acoustics Branch, AIAA Associate Fellow.
†Senior Research Scientist, Research Directorate, Computational AeroSciences Branch, AIAA Associate Fellow.
‡Senior Research Scientist, Research Directorate, Structural Acoustics Branch, AIAA Associate Fellow.
§Research Scientist, Research Directorate, Structural Acoustics Branch, AIAA Senior Member.

The threefold purpose of the current study is (1) to evaluate the effects of CMC material on the acoustic performance of liners, (2) to evaluate the broadband absorptive properties of variable-depth liners, and (3) to assess the ability of two propagation codes to predict the acoustic performance of variable-impedance liners.

The effects of the CMC material porosity are explored via tests in the Normal Incidence Tube (NIT) and Grazing Flow Impedance Tube (GFIT). Also, liners constructed via stereolithography are tested in the GFIT to gain additional insight into the effects of material porosity. The SLA process is chosen because the resultant material exhibits a negligible porosity, similar to that found in conventional liner materials. GFIT tests are also used to explore the ability to achieve broadband noise reduction via variable-depth liners, and to determine whether the orientation of these liners can be used to improve this noise reduction. Finally, two propagation codes[2,3] are used to predict the acoustic pressure profile of the SLA variable-depth liner. For the sake of brevity, the data presented herein do not include the effects of mean flow.

Section II provides a description of the experimental methods used to evaluate the liner configurations, and also provides a description of each of the test liners used in this study. The impedance prediction model is provided in Section III, and the acoustic propagation models are described in Section IV. Key results are provided in Section V, and concluding remarks are presented in Section VI.

II. Experimental Method

A. Test Rigs

Two test rigs are used in this study, the Normal Incidence Tube (NIT) and the Grazing Flow Impedance Tube (GFIT). The NIT is used to determine the normal incidence acoustic impedance of single-degree-of-freedom (SDOF) liners constructed with CMC material. The GFIT is used to evaluate the acoustic performance of three test liners, one constructed with CMC material and two constructed via an SLA process.

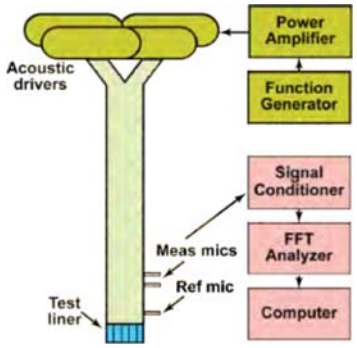

Figure 1: Sketch of NASA Normal Incidence Tube (NIT).

1. *Normal Incidence Tube (NIT)*

The NIT is a 50.8 mm × 50.8 mm waveguide (Fig. 1). It contains six 120-W compression drivers to generate a plane-wave sound field that impinges on the surface of the liner and combines with reflections from the liner to create a standing wave pattern. The Two-Microphone Method (TMM)[4,5] is used to measure the complex acoustic pressures at two prescribed distances from the liner surface, such that the frequency dependence of the acoustic impedance of the liner can be computed. Tonal tests (one frequency at a time) are conducted for source frequencies of 0.4 to 3.0 kHz in 0.2 kHz increments, with source sound pressure levels (SPLs) of 120 and 140 dB at the reference microphone. A computer-controlled function generator is used to generate these tones. Two amplitudes are used so that test liner nonlinearities can be evaluated by determining whether the impedance is a function of the source SPL.

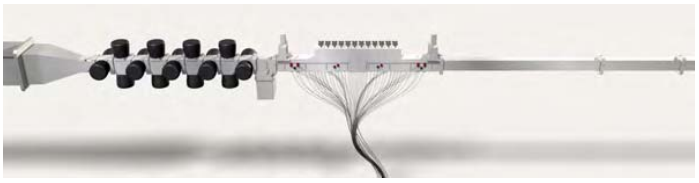

Figure 2: Sketch of Grazing Flow Impedance Tube (GFIT).

2. Grazing Flow Impedance Tube (GFIT)

The GFIT has a cross-sectional geometry of 50.8 mm wide by 63.5 mm high, such that higher-order modes in the horizontal and vertical dimensions cut on at different frequencies. It allows evaluation of acoustic liners with lengths from 50.8 mm to 609.6 mm. The surface of the test liner forms a portion (406.4 mm for the current investigation) of the upper wall of the flow duct. For the current investigation, the source section consists of twelve acoustic drivers mounted upstream (exhaust mode) of the test section. (Fig. 2 shows an earlier configuration with eighteen drivers.) These drivers were used to generate tones (one frequency at a time) at 130 dB over a frequency range of 0.4 to 3.0 kHz. These tests were conducted with no mean flow.

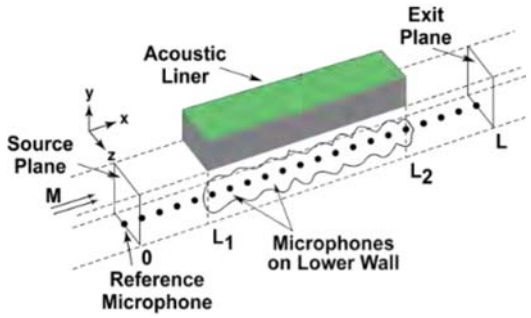

Figure 3: Sketch of Grazing Flow Impedance Tube test section.

Fifty-three microphones flush-mounted in the lower wall (opposite the liner) are used to measure the acoustic pressure field over the axial extent of $0 \leq x \leq L$ (see Fig. 3). For each data acquisition, 1000 averages on each microphone channel (1024 data points per average) are taken. A cross-spectrum signal extraction method[6] is used to determine the amplitudes and phases at each of the microphone locations relative to the amplitude and phase at the reference microphone location.

B. Test Liners

Figure 4 provides photographs of the CMC liners tested in the NIT and GFIT. The facesheet for each of these liners is 0.8 mm thick, and contains 1.0 mm-diameter orifices to achieve a facesheet porosity of approximately 5.5%. It should be noted that each of the CMC liners (four NIT and one GFIT sample) was fabricated as a single unit (perforated facesheet, honeycomb core, and back plate). Thus, the cross-sectional dimensions of the core chambers could not be ascertained without partially destroying a liner. However, based on inspection of the outer edges of these liners, the NIT samples contain approximately 9 core chambers with nominal cross-sectional dimensions of 15 mm $\times$ 15 mm. The GFIT liner has approximately 69 core chambers with the same cross-sectional dimensions.

Four SDOF liners (see Fig. 4-a) were fabricated for testing in the NIT, with constant depths of 152.4, 76.2, 25.4, and 12.7 mm, respectively. These depths were chosen to evaluate the validity of the impedance prediction model over a range of channel depths that might be considered for use in core-noise liners. A

406.4 mm-long, variable-depth CMC liner (see Fig. 4-b) was constructed for testing in the GFIT. The core depth for this liner varies from 76 to 14 mm. This liner was tested with two orientations, first with the smallest cavity depths at the leading edge, then with the largest cavity depths at the leading edge.

It should be noted that this GFIT liner has some features that are not captured in the current impedance prediction model (presented in Section III). First, it has a perforated sheet (see Fig. 4-b) at the lower surface of the core. Thus, although a rigid back plate is added beneath this perforated sheet when the liner is placed into the holder, the boundary condition at the lower surface of the liner core should be modeled as a compliant surface, and not as a rigid back plate. Second, the core chambers in this liner are not perpendicular to either surface (upper or lower) of the liner. Finally, the partitions between adjacent core chambers cause full or partial blockage of a number of the orifices in the facesheet, and therefore add uncertainty to the estimate of facesheet porosity.

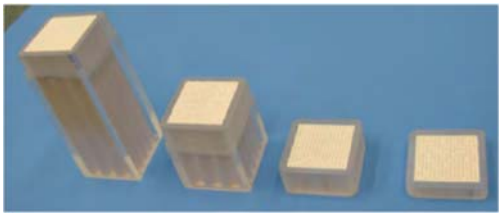

(a) Constant-depth liners (152.4, 76.2, 25.4, and 12.7 mm) tested in the NIT.

(b) Variable-depth liner tested in the GFIT, with holder.

Figure 4: Photographs of CMC liners.

To avoid confusion, it is important to draw attention to the fact that two independent types of porosity are of interest for the CMC liners. The first is the facesheet porosity (approximately 5.5%), which is computed as the ratio of the combined area of all of the 1 mm-diameter orifices to the total surface area of the liner. This porosity is independent of the type of material used in the construction of the liner. The second porosity has to do with the CMC material. Due to the way in which the CMC material is constructed, the resultant structure has a porosity of approximately 20%. However, whereas the facesheet orifices are clearly visible, the pores in the CMC material are not. As such, the expectation is that these pores have diameters that are small enough that they do not affect the acoustic performance of liners constructed with this material. By comparison, the material used in the SLA process has a negligible porosity.

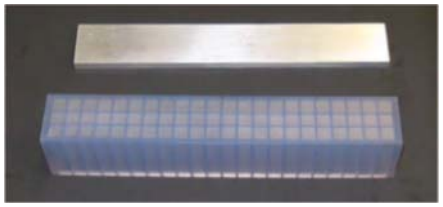

(a) Constant-depth liner with back plate.

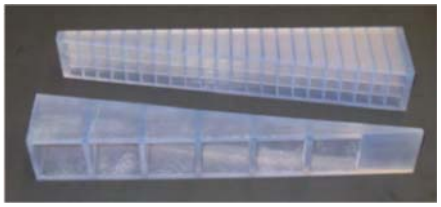

(b) Variable-depth liner with back plate.

Figure 5: Photographs of constant-depth and variable-depth perforate-over-honeycomb liners constructed via an SLA process.

Two additional liners (see Fig. 5) were fabricated for evaluation in the GFIT using an SLA process. The perforate facesheet and core chambers were fabricated as a single piece for both liners. The back plates for these liners were fabricated separately, such that excess material used in the fabrication process could be easily removed from the main body of each liner. The facesheet for each liner has a porosity of 5.5%, a thickness of 0.8 mm, and an orifice diameter of 1.0 mm. The core depth of the first liner is 76.2 mm. Thus, this liner is tuned for optimum sound reduction at a single frequency. The second is a variable-depth

liner with nearly identical geometric dimensions as the CMC variable-depth liner. The core depth for this liner varies from 15.2 to 74.6 mm. For both SLA liners, the core chambers are 15.2 mm $\times$ 15.2 mm, and are separated by 2.5 mm-wide partitions. There are 22 core chambers in the axial dimension, and 3 core chambers in the spanwise dimension, for a total of 66 core chambers in each liner.

III. Impedance Prediction Model

A transmission line model for predicting the surface acoustic impedance of an individual liner chamber is briefly described herein with the aid of Fig. 6. This figure provides a sketch of a single chamber of a liner with an air gap with height h_1 and a perforate sheet with thickness h_2. Each unique portion of the liner chamber is treated separately. In the ensuing discussion, these unique portions (air gaps or perforated sheet) are treated as individual "computational layers."

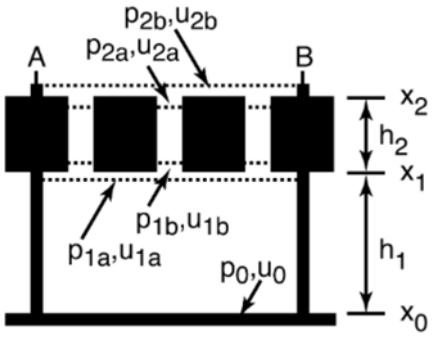

Figure 6: Sketch of single chamber with key parameters for transmision line impedance prediction model.

The computation is initiated by assuming the backplate at x_0 to be rigid and impervious. The acoustic pressure and particle velocity are given as

$$\begin{pmatrix} p_0 \\ u_0 \end{pmatrix} = \begin{pmatrix} 1 \\ 0 \end{pmatrix} \tag{1}$$

which yields an infinite impedance at this location. All acoustic pressures and particle velocities are normalized by ρc^2 and c, respectively, where the density of the air, ρ, and the speed of sound, c, are for the prevailing static pressure and air temperature. Changes in the acoustic pressure and particle velocity across a computational layer are computed via

$$\begin{pmatrix} p_{n+1} \\ u_{n+1} \end{pmatrix} = \begin{bmatrix} T_{11} & T_{12} \\ T_{21} & T_{22} \end{bmatrix} \begin{pmatrix} p_n \\ u_n \end{pmatrix} \tag{2}$$

where the transmission coefficients (T_{11}; T_{12}; T_{21} and T_{22}) depend on the type of layer (air gap or perforate sheet) being considered.

For transmission through a duct filled with air, the transmission coefficients are given by

$$T_{11} = T_{22} = \cosh(k\Gamma h);\ T_{12} = \zeta_c \sinh(k\Gamma h);\ T_{21} = \zeta_c^{-1} \sinh(k\Gamma h) \tag{3}$$

where $k = \omega/c$ is the free-space wavenumber, ω is the angular frequency, and h is the layer thickness. Also, impedances are normalized by the characteristic impedance of air, ρc. The propagation constant, Γ, and characteristic impedance, ζ_c, are computed as

$$\Gamma = \sqrt{\frac{J_0(i^{3/2}s)}{J_2(i^{3/2}s)}}\sqrt{\frac{\sigma}{n_\sigma}}; \qquad \zeta_c = \frac{-i}{\sigma}\frac{J_0(i^{3/2}s)}{J_2(i^{3/2}s)}; \qquad n_\sigma = \sqrt{1 + \frac{\sigma - 1}{\sigma}\frac{J_0(i^{3/2}\sigma s)}{J_0(i^{3/2}s)}}^{\sigma\sigma 1} \tag{4}$$

where $i = \sqrt{-1}$ is the imaginary unit, $s = (d_c/2)\sqrt{\rho_s \omega/\mu}$ is the shear wave number, J_m is the Bessel function of order m, and d_c, ρ_s, ω, μ, σ^2 and γ are the channel diameter, static density, angular frequency, coefficient of viscosity, Prandtl number and specific heat ratio, respectively. Application of Eqns. 1 - 4 to the liner core chamber shown in Fig. 6 yields acoustic pressure and particle velocity at the lower surface of the perforated sheet, depicted as p_{1a} and u_{1a}, respectively.

The acoustic pressure and acoustic mass flow are assumed constant across the {1a; 1b} interface,

$$p_{1b} = p_{1a}; \qquad N S_{1b} u_{1b} = S_{1a} u_{1a} \tag{5}$$

where N is the number of orifices (3 in this example) connected to a single air cavity, S_{1a} is the cross-sectional area at the top of the air cavity (denoted by the long dashed line at the top of the cavity) and S_{1b} is the cross-sectional area within a single perforate orifice. Next, the wave propagation within the single orifice is computed using Eqs. 2 and 3, where the orifice diameter is used as the "channel diameter." Again, the acoustic pressure and acoustic mass flow are assumed to be constant across the {2a; 2b} interface (denoted by the dashed line with endpoints A and B), such that

$$p_{2b} = p_{2a}; \qquad S_{2b} u_{2b} = N S_{2a} u_{2a} \tag{6}$$

The normalized surface impedance for the chamber is computed as

$$\zeta_{ch} = \frac{p_{2b}}{u_{2b}} \tag{7}$$

and the surface impedance spectra of the individual chambers are combined to compute the effective impedance across the liner surface. For this computation, it is preferable to use acoustic admittance ($\beta_{ch} = 1/\zeta_{ch}$). The effective admittance across a selected extent of liner surface is given by

$$\beta_s = \sigma \sum_{i=1}^{N_{ch}} \beta_{ch} \tag{8}$$

where N_{ch} represents the number of chambers that combine to form the liner and σ is the surface open area ratio (porosity) of the liner. The uniform, effective, surface impedance of the liner is then given by $\zeta_s = 1/\beta_s$.

IV. Acoustic Propagation Codes

Results from two acoustic propagation codes, CDUCT-LaRC (CDL) and Q3D-FEM, are used to compare with the data acquired in the GFIT. Each of these codes has been described in detail in earlier publications. Thus, for the sake of brevity, the following discussion is limited to a description of those features that are of particular importance to the current investigation. Both codes assume the liner to be installed on the upper wall (as in the GFIT) and allow the impedance to vary along the axial length of the liner. As mentioned earlier, the results presented herein are for the no-flow condition.

The CDL propagation code[7] utilizes a parabolic approximation to the convected Helmholtz equation and is a computationally efficient model that accounts for fully three-dimensional geometries. The parabolic approximation neglects reflections due to impedance discontinuities at the leading ($x = L_1$) and trailing ($x = L_2$) edges of the liner (see Fig. 3). Similarly, the termination at $x = L$ is assumed to be anechoic.

The Q3D-FEM propagation code[8] uses a finite element model of the convected Helmholtz equation. This elliptical model includes the effects of reflections at the leading and trailing edges of the liner. It also allows for inclusion of the effects of reflections at the termination. This code is typically used as the basis for the NASA impedance eduction method[9,10] based on acoustic pressure data acquired in the GFIT. When used for impedance eduction in the current study, the effects of reflections at the termination plane are included in Q3D-FEM. On the other hand, when the Q3D-FEM code is used to predict sound transmission through the GFIT (for comparison to measured data or to predictions via the CDL code), the termination is assumed to be anechoic.

V. Results and Discussion

The first goal of the current study is to evaluate the effects of CMC material porosity on the acoustic performance of liners. The initial evaluation is based on tests conducted in the NIT for four constant-depth CMC liners. Representative results for CMC liners with core depths of 25.4 and 152.4 mm, respectively, are provided in Figure 7. Similar results were achieved with the other two core depths. This figure provides a comparison of predicted (lines) and measured (symbols) normal incidence impedance spectra, □ = □ + i □. The predictions are based on the impedance prediction model described in Section III, and the measurements were acquired via the TMM in the NIT. Although there are slight discrepancies, the comparison is generally quite good, even capturing the effects of increased resistance at frequencies near anti-resonance.

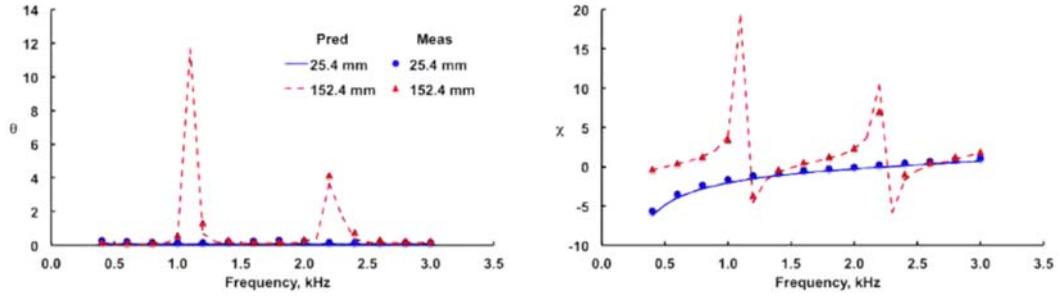

(a) Normalized resistance.

(b) Normalized reactance.

Figure 7: Normal incidence impedance, □ = □ + i □, for two single-degree-of-freedom CMC liners.

Recall that the same CMC material is used for the facesheet and interior partitions of the CMC liners. For NIT measurements, the fact that the interior partitions (between adjacent core chambers) are porous is not important, as the impinging normal-incidence sound field is planar, i.e., the phase of the incident acoustic wave is constant across the surface of the liner. However, the same is not true for the facesheet, because the impedance prediction model assumes the facesheet porosity to be solely due to the 1 mm-diameter orifices, i.e., the effects of material porosity (reminder - this is not referring to the porosity of the facesheet due to the 1 mm-diameter orifices) are not included in the model. Thus, the favorable comparisons shown in Fig. 7 indicate the effects of material porosity on the measured impedance are negligible when the liner is exposed to normal-incidence sound.

However, acoustic liners are typically mounted in the walls of flow ducts (e.g., engine nacelle aft-bypass duct), and are exposed to grazing-incidence sound and flow. GFIT tests are used to evaluate acoustic liners in this environment. For this implementation, the phase of the sound entering adjacent core chambers (via orifices in the facesheet) is not constant, as the phase changes along the axial length of the duct. If the interior partitions are sufficiently porous, the liner will not behave as a local-reaction liner, but will instead exhibit extended-reaction liner behavior. As a result, the attenuation achieved by the liner will not be accurately predicted via a local-reaction impedance prediction model. Ideally, a constant-depth CMC liner would be tested in the GFIT, and the measured frequency-dependent SPL profiles would be compared with corresponding predicted SPL profiles to determine whether the material porosity of the interior partitions affects the ability to predict the acoustic performance of the liner. For the current study, however, a constant-depth CMC liner was not available for evaluation in the GFIT.

Instead, a two-part approach is adopted to evaluate material porosity effects. First, two SLA liners were constructed, one with a constant depth and the other with a variable depth similar to that of the CMC liner. These SLA liners have negligible material porosity, and their acoustic performance is therefore expected to be well predicted via the acoustic propagation codes (see Sec. IV) with the liners represented as impedance boundary conditions (see Sec. III). Next, measured acoustic pressure profiles acquired for the CMC and SLA variable-depth liners are compared. Since the geometric parameters of these two liners are

nearly identical, the respective acoustic pressure profiles should be very similar if the material porosity is not causing deleterious effects. If this is demonstrated to be true, it suggests the impedance prediction model should also be suitable to determine the axially varying impedance of variable-depth liners constructed with this CMC material. In addition, a comparison of attenuations achieved via the CMC and SLA variable-depth liners is used to demonstrate broadband noise reduction capability.

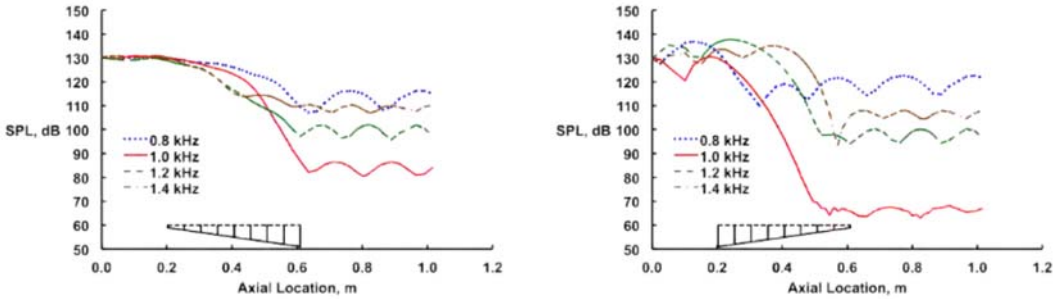

(a) Small depth at liner leading edge.

(b) Large depth at liner leading edge.

Figure 8: Axial acoustic pressure profiles measured with variable-depth CMC liner mounted in GFIT.

Figure 8 provides a comparison of axial acoustic pressure profiles, SPL(x), acquired in the GFIT with the array of microphones flush-mounted in the wall opposite the variable-depth CMC liner. The GFIT is configured in the exhaust configuration (sound source located upstream of the test liner, at x < 0) and there is no flow (Mach 0.0). The measured data are provided at frequencies of 0.8, 1.0, 1.2 and 1.4 kHz. For all of the cases presented in this paper, the frequency at which maximum attenuation occurs is within this frequency range. Clearly, the orientation (see liner sketch at bottom of graph) of the liner has an effect on the axial distribution of sound absorption that is produced by the liner. For all but the 1.0 kHz case, the total amount of attenuation (i.e., difference in SPLs at x = 0:00 m and x = 1:02 m) is similar for each liner orientation. At 1.0 kHz, however, positioning the large depth at the leading edge (LE) of the liner results in approximately 17 dB more attenuation than is achieved when the large depth is at the trailing edge (TE).

An interesting feature of Fig. 8 is the presence of significant standing wave patterns at the upstream end of the liner when the large depth is at the LE. When the liner orientation is reversed, this feature is virtually eliminated. This illustrates that the larger LE impedance discontinuity (for the frequencies that are shown) for the configuration with the large-depth chambers at the LE (Fig. 8-b) has a significant effect on the acoustic pressure profile. Indeed, the large depth (76.2 mm) is tuned for a resonant frequency of approximately 1.0 kHz, whereas the small depth (14.0 mm) is tuned for a resonant frequency near 6.0 kHz.

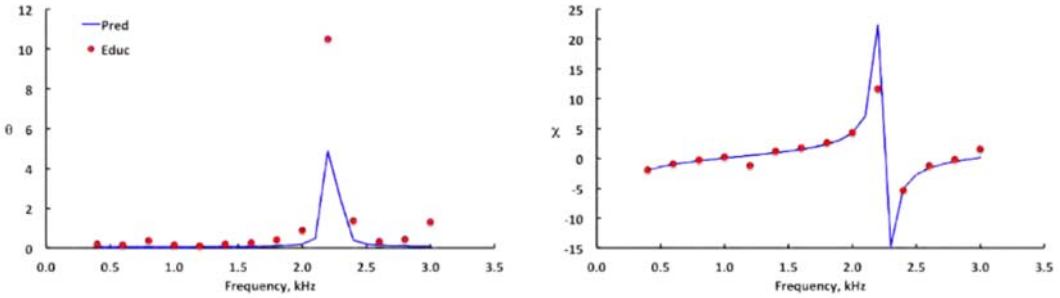

(a) Normalized resistance.

(b) Normalized reactance.

Figure 9: Comparison of predicted and educed acoustic impedance spectra for the constant-depth SLA liner.

The next series of GFIT tests was conducted with the SLA liners described in Section II.B. The constant-depth liner was tested first, and the resultant data were used with the impedance eduction method to determine the acoustic impedance at the surface of the liner. Also, the geometric parameters of this liner were used as input to the impedance prediction model to determine the predicted acoustic impedance. Fig. 9 provides a comparison of the resultant predicted and educed impedance spectra. As was observed for the NIT data (Fig. 7), the comparison is quite favorable. This lends confidence that the current impedance prediction model is suitable for predicting the axially varying impedance spectra due to varying chamber depths along the extent of the variable-depth SLA liner.

The data acquired with the SLA liners were also used to validate two propagation codes, CDL and Q3D-FEM. Figures 10 - 12 provide a comparison of measured and predicted acoustic pressure profiles, $\mathsf{SPL(x)}$, for the variable-depth SLA liner. Data were acquired in the GFIT with the liner mounted in two orientations (see Fig. 10). The small-depth chambers were located at the LE of the liner for Orientation 1, and at the TE of the liner for Orientation 2. The geometrical dimensions (e.g., orifice diameter, porosity) were used with the impedance prediction model to estimate the impedance spectra at multiple axial locations along the surface of the liner. These predictions were made at the axial locations corresponding to the center of each core chamber (22 locations). These impedance spectra were then used as input to the propagation codes (CDL and Q3D-FEM) such that the corresponding acoustic pressure profiles could be predicted. The results of these predictions are provided in Fig. 11 for the CDL code, and in Fig. 12 for the Q3D-FEM code.

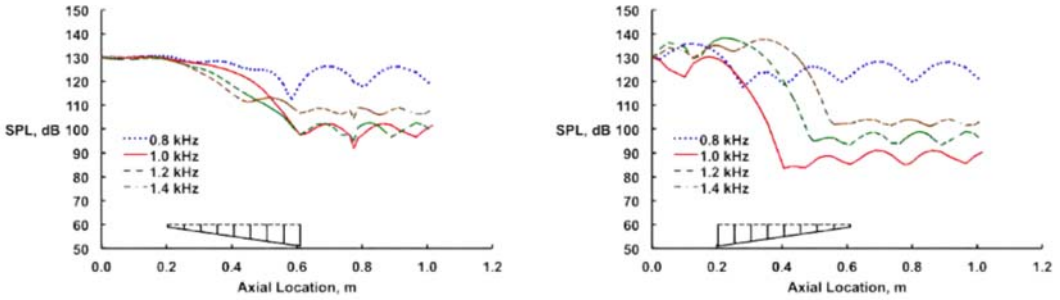

(a) Orientation 1 - small-depth chambers at LE.

(b) Orientation 2 - large-depth chambers at LE.

Figure 10: Measured SPL(x) for variable-depth SLA liner; two orientations.

The measured data demonstrate significant effects of liner orientation. When the small-depth chambers are at the leading edge (LE) of the liner, minimal reflections are observed at the LE. For these frequencies, the small-depth chambers present a surface impedance that is nearly the same as a hard wall condition, and the impedance gradually transitions toward optimum as the chamber lengths increase along the axial extent of the liner. When the orientation is reversed, significant reflections occur at the LE. For this orientation, the impedance presented at the LE is at or near optimum (for the frequencies considered), i.e., very different from the upstream hard wall boundary condition. This discontinuity in the surface impedance is the cause of the upstream standing waves. The total attenuation ($\mathsf{SPL(1{:}02\,m) - SPL(0\,m)}$) is also much greater when the large-depth chambers are placed at the liner LE.

Finally, it is of interest to note the shape of the acoustic pressure profiles for the different orientations. For convenience, we focus on the data acquired at 1.0 kHz, the frequency of maximum attenuation. For the first orientation (small depths at LE), the SPL begins to gradually reduce as the sound approaches the portion of the liner that is optimally tuned for this frequency. As the sound passes over this "optimally tuned" portion of the liner, the slope of the sound reduction becomes noticably larger. After the sound passes the trailing edge (TE) of the liner, the acoustic pressure profile flattens and becomes dominated by a standing wave pattern due to a non-anechoic termination at the downstream end of the GFIT. For the second orientation (large depths at LE), the portion of the liner that is optimally tuned for 1.0 kHz occurs near the LE. Hence,

the slope of sound reduction is large at this location. However, it is particularly interesting to note that this large slope continues over the entire first half of the liner before the acoustic pressure profile becomes dominated by the downstream standing wave pattern.

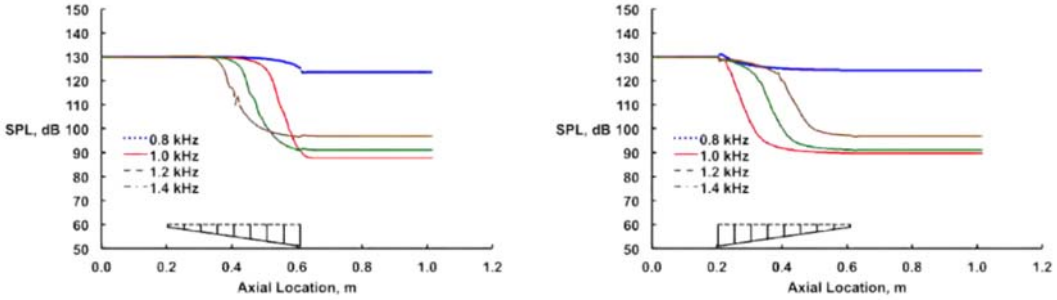

(a) Orientation 1 - small-depth chambers at LE.

(b) Orientation 2 - large-depth chambers at LE.

Figure 11: Predicted SPL(x) for the variable-depth SLA liner using CDL; two orientations.

Figure 11 provides the acoustic pressure profiles for the same four frequencies using the CDL propagation code. Comparison with the measured profiles presented in Fig. 10 yields a few points of interest. Recall that the parabolic approximation does not allow for reflections, i.e., all of the energy is forced into forward-propagating modes. As a result, no standing waves are observed, either at the LE of the liner or at the termination of the duct. In spite of this simplification, there are many similarities to the measured data. The predicted attenuations for the selected test frequencies follow the same trends as the measured data, but the predicted attenuations tend to be conservative. Also the axial location where the sound begins to decay for each test frequency is quite similar to that observed in the measured data.

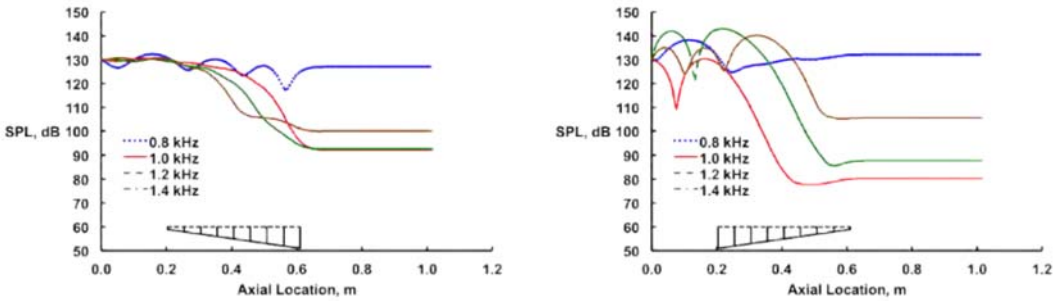

(a) Orientation 1 - small-depth chambers at LE.

(b) Orientation 2 - large-depth chambers at LE.

Figure 12: Predicted SPL(x) for the variable-depth SLA liner using Q3D-FEM; two orientations.

Figure 12 provides the corresponding acoustic pressure profiles predicted using the Q3D-FEM propagation code. As this code employs an elliptical approach, reflections at the LE of the liner are included. Thus, the effects of orientation noted with the measured profiles are also present in these predictions. These include (1) minimal standing waves upstream of the liner LE for Orientation 1, (2) significant standing waves at this location for Orientation 2, (3) locations of onset of sound decay for the selected frequencies, and (4) slope of the sound decay for these frequencies. As these predictions were made independent of the measured data, the effects of the non-anechoic termination were not included. This causes the predictions to become flat at the

TE of the liner. However, the predicted acoustic pressure profiles upstream of the liner TE are remarkably similar to the corresponding measured profiles.

Overall, the results achieved with the variable-depth SLA liner suggest that either of the two propagation codes can be used to predict the acoustic pressure profiles of this type of liner. The lower-fidelity CDL code is more than sufficient for comparative studies of this type of variable-impedance liner, and can therefore be used with confidence to downselect liner configurations for further investigation. The higher-fidelity Q3D-FEM code can then be used to study the selected configurations in greater detail.

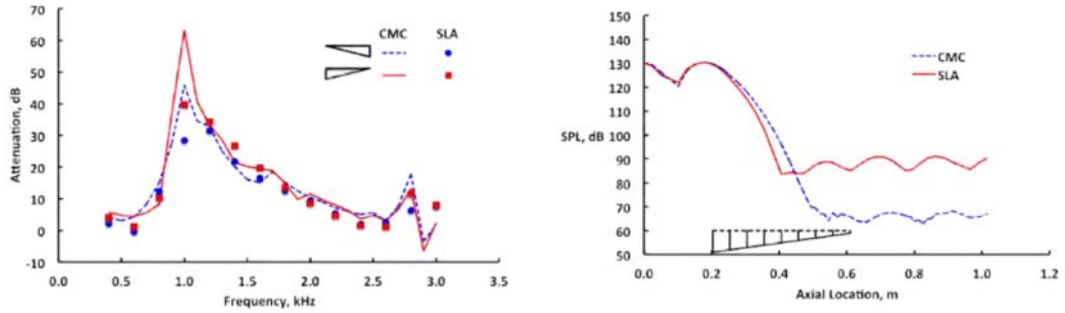

(a) Measured attenuation; two orientations.

(b) Measured SPL(x), large-depth chambers at LE.

Figure 13: Comparison of CMC and SLA variable-depth liners.

The last point of interest is a comparison of the measured acoustic profiles for the CMC (Fig. 8) and SLA (Fig. 10) variable-depth liners. Figure 13 provides a comparison of data measured with these two samples. The attenuations ($\mathsf{SPL(L) - SPL(0)}$, where $\mathsf{L = 1{:}0}$ m) observed for the two variable-depth liners (both liner orientations) are shown in Fig. 13-a. Since the SLA liner was designed to be nearly identical to the CMC liner, their respective acoustic pressure profiles and resultant attenuations would be expected to be very similar. In general, the profiles are observed to be similar for all but the optimum frequency (1.0 kHz). However, an additional 23 dB of sound decay is observed at this frequency for the CMC liner (see Fig. 13-b). There are a number of possible explanations. As mentioned earlier, the material porosity is much larger for the CMC material than for the SLA material. Also, the compliance of the respective materials may be different. However, it is noted that the results are very similar at all but the optimum frequency. This suggests that material differences are not the cause of the difference at the optimum frequency, as the effects of those differences would not be expected to be confined to a single frequency. Instead, a more likely cause for the differences at this frequency is the geometry of the two liners. Recall that the core depths for the two liners are slightly different. Also, a number of the facesheet orifices in the CMC liner are fully or partially blocked, whereas all of the orifices in the SLA liner are fully open. Finally, the inclusion of a perforate sheet at the lower surface of the CMC liner core causes a change in the impedance. In summary, although the geometries of the two liners are very similar, they are not identical. Thus, the geometry of the CMC liner is believed to be slightly better optimized for attenuation of the 1.0 kHz tone. Regardless, the results clearly demonstrate that CMC material is suitable for use in acoustic liners. They also demonstrate that variable-depth liner configurations can be used to achieve significant broadband noise reduction.

VI. Concluding Remarks

A series of tests has been conducted in the NASA Langley Normal Incidence Tube (NIT) and Grazing Flow Impedance Tube (GFIT) to evaluate acoustic liners constructed using ceramic matrix composite (CMC) material. Additional GFIT tests were conducted with samples fabricated using a stereolithography (SLA) process. For this study, all tests and predictions were for the no-flow condition. The resultant data are used to draw the following conclusions:

1. The surface impedance spectra of four constant-depth CMC samples were determined using data acquired in the NIT. Corresponding impedance spectra were predicted for each sample based on their respective geometries. The predicted and measured impedance spectra compare favorably, indicating liners constructed with CMC material can be properly modeled via the current impedance prediction model.

2. GFIT tests with CMC and SLA variable-depth liners show significant effects of sample orientation. Specifically, if the impedance gradually changes from a hard wall condition to the optimum impedance for sound absorption, minimal standing waves are present at the leading edge of the liner. On the other hand, the opposite is true if the liner orientation is reversed such that the impedance discontinuity at the liner leading edge is more pronounced. Both orientations produce significant sound absorption over a broad frequency range, but the latter orientation results in the maximum attenuation for this liner.

3. A constant-depth SLA liner was tested in the GFIT, and the resultant data were used to educe the impedance of this liner. Separately, the liner geometry was used to predict the surface impedance of the liner. These educed and predicted impedance spectra are observed to compare favorably. Hence, the impedance prediction model is determined to be suitable for use with similarly constructed liners.

4. A variable-depth SLA liner was constructed with similar geometry to that of the variable-depth CMC liner, such that a comparison of acoustic pressure profiles acquired in the GFIT could be used to evaluate the effects of the respective material properties on the sound absorption. In general, this comparison shows very similar results, thereby implying the material properties of the CMC liner have no significant effect on the resultant sound absorption.

5. Two acoustic propagation codes were used to compare with acoustic pressure profiles measured in the GFIT. The first (CDL) uses a parabolic approximation to the convected Helmholtz equation, and the second (Q3D-FEM) uses an elliptical model of the same equation. The CDL code shows similar trends to the measured data for the variable-depth SLA liner, whereas the higher-fidelity Q3D-FEM code is able to predict more of the finer detail present in the measured data. These results suggest the CDL code can be used with confidence for downselect of liner configurations, and the Q3D-FEM code can be used for more detailed investigations, at least for the no-flow condition.

This investigation has also demonstrated some of the potential for sound absorption with acoustic liners for which the impedance is varied along the length of the liner. A number of interesting features were observed, some of which suggest significant improvements might be achievable via properly designed, variable-depth liners. Further evaluation of this concept will be the focus of future investigations.

Acknowledgments

The authors would like to express appreciation to Carol Harrison and Martha Brown of NASA Langley Research Center and Jerry Lyle of Northrop Grumman for assistance in the testing, and to Doug Kiser and Lennart Hultgren of NASA Glenn Research Center for contributions regarding the CMC liner portion of this study. The Fixed Wing Project of NASA's Fundamental Aeronautics Program funded this work.

References

[1]Lockard, D. P. and Lilley, G. M., "The Airframe Noise Reduction Challenge," NASA TM 213013, 2004.

[2]Nark, D. M., "Assessment of Radiated Fan Noise Prediction Capabilities using Static Engine Test Data," AIAA Paper 2011-2807, June 2011.

[3]Watson, W. R. and Nark, D. M., "Assessment of NASA's Aircraft Noise Prediction Capability, Chapter 6: Assessment of Acoustic Propagation and Radiation Codes for Locally Reacting Liners in Flow Ducts," NASA TP 2012-215653, July 2012.

[4]Chung, J. Y. and Blaser, D. A., "Transfer function method of measuring in-duct acoustic properties: I. Theory," Journal of Acoustical Society of America, Vol. 68, 1980, pp. 907–921.

[5]Jones, M. G. and Parrott, T. L., "Evaluation of a multi-point method for determining acoustic impedance," Journal of Mechanical Systems and Signal Processing, Vol. 3, No. 1, 1989, pp. 15–35.

[6]Bendat, J. S. and Piersol, A. G., Random Data: Analysis and Measurement Procedures, Wiley-Interscience, 1971.

[7]Nark, D. M. and Jones, M. G., "Broadband Liner Optimization for the Source Diagnostic Test Fan," AIAA Paper 2012-2195, June 2012.

[8]Watson, W. R., Jones, M. G., and Parrott, T. L., "Validation of an Impedance Eduction Method in Flow," AIAA Journal, Vol. 37, No. 7, June 1998, pp. 818–824.

[9]Watson, W. R. and Jones, M. G., "Comparison of Convected Helmholtz and Euler Model for Impedance Eduction in Flow," AIAA Paper 2006-2643, May 2006.

[10]Jones, M. G., Watson, W. R., Tracy, M. B., and Parrott, T. L., "Comparison of Two Waveguide Methods for Educing Liner Impedances in Grazing Flow," AIAA Journal, Vol. 42, No. 2, Februrary 2004, pp. 232–240.